

Lawrence Berkeley National Laboratory

Recent Work

Title

TEST OF TIME REVERSAL INVARIANCE AND MEASUREMENTS OF POSITION AND NEUTRINO ASYMMETRIES IN POLARIZED ^{19}Ne BETA DECAY

Permalink

<https://escholarship.org/uc/item/1vv7q5f1>

Authors

Calaprice, Frank P.
Commins, Eugene D.
Gibbs, Hyatt M.
et al.

Publication Date

1969-01-15

RECEIVED
LAWRENCE
RADIATION LABORATORY

MAR 24 1969

LIBRARY AND
DOCUMENTS SECTION

UCRL-18647

ey. J

TEST OF TIME REVERSAL INVARIANCE AND
MEASUREMENTS OF POSITRON AND NEUTRINO
ASYMMETRIES IN POLARIZED ^{19}Ne BETA DECAY

Frank P. Calaprice, Eugene D. Commins,
Hyatt M. Gibbs, Gerald L. Wick, and David A. Dobson

January 15, 1969

TWO-WEEK LOAN COPY

This is a Library Circulating Copy
which may be borrowed for two weeks.
For a personal retention copy, call
Tech. Info. Division, Ext. 5545

LAWRENCE RADIATION LABORATORY
UNIVERSITY of CALIFORNIA BERKELEY

UCRL-18647

ey. J

DISCLAIMER

This document was prepared as an account of work sponsored by the United States Government. While this document is believed to contain correct information, neither the United States Government nor any agency thereof, nor the Regents of the University of California, nor any of their employees, makes any warranty, express or implied, or assumes any legal responsibility for the accuracy, completeness, or usefulness of any information, apparatus, product, or process disclosed, or represents that its use would not infringe privately owned rights. Reference herein to any specific commercial product, process, or service by its trade name, trademark, manufacturer, or otherwise, does not necessarily constitute or imply its endorsement, recommendation, or favoring by the United States Government or any agency thereof, or the Regents of the University of California. The views and opinions of authors expressed herein do not necessarily state or reflect those of the United States Government or any agency thereof or the Regents of the University of California.

Submitted to The Physical Review

UCRL-18647
Preprint

UNIVERSITY OF CALIFORNIA

Lawrence Radiation Laboratory
Berkeley, California

AEC Contract No. W-7405-eng-48

TEST OF TIME REVERSAL INVARIANCE AND MEASUREMENTS OF POSITRON
AND NEUTRINO ASYMMETRIES IN POLARIZED ^{19}Ne BETA DECAY

Frank P. Calaprice, Eugene D. Commins, Hyatt M. Gibbs,
Gerald L. Wick, and David A. Dobson

January 15, 1969

TEST OF TIME-REVERSAL INVARIANCE
AND MEASUREMENTS OF POSITRON AND NEUTRINO ASYMMETRIES
IN POLARIZED ^{19}Ne BETA DECAY*

Frank P. Calaprice, Eugene D. Commins, Hyatt M. Gibbs[†], and Gerald L. Wick[‡]

Department of Physics and Lawrence Radiation Laboratory
University of California, Berkeley, California

and

David A. Dobson[‡]

Lawrence Radiation Laboratory, Livermore, California

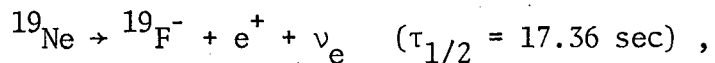
ABSTRACT

We present a comprehensive discussion of an experiment, previously reported, to test time-reversal (T) invariance in the beta decay of ^{19}Ne . The "time-reversal" coefficient D as well as the neutrino and positron asymmetry coefficients B and A, respectively, are measured, with results as follows: $D = +0.002 \pm 0.014$, $B = -0.90 \pm 0.13$, and $A = -0.039 \pm 0.002$. The value of D, based on 30000 events, is consistent with T invariance. The latter implies $D = 0$, since final-state corrections to D are negligible.

The atomic-beam method is used to form a nuclear-spin polarized beam of ^{19}Ne atoms in the 1S_0 ground state. Coefficients D and B are measured by observing correlations between the positron and recoil ion $^{19}\text{F}^-$ (in delayed coincidence) with respect to the ^{19}Ne spin polarization, from decays in flight. The beam terminates its flight in a cell, where ^{19}Ne atoms are captured and remain for approximately 3 seconds, but suffer no significant depolarization. Positrons emitted parallel and antiparallel to the spin by ^{19}Ne decaying in the cell are counted to measure A. The results of our measurements are compared with similar observations of the beta decay of polarized neutrons.

I. INTRODUCTION

We present here a detailed report of a test for time-reversal (T) invariance in the allowed beta decay



provided by search for a correlation of the form $\underline{J} \cdot \underline{p}_e \times \underline{p}_\nu$ between the spin of the initial nucleus and the momenta of the final leptons.¹ The experiment consists in forming a polarized atomic beam of ${}^{19}\text{Ne}$ and correlating the nuclear polarization with coincidences between the positrons and recoil ions, ${}^{19}\text{F}^-$, from decays in flight. The positron asymmetry parameter "A" and the neutrino asymmetry parameter "B" are also measured. Similar experiments have been carried out on beta decay of polarized neutrons.²⁻⁴

Our work was motivated by the discovery of CP violation in K_2^0 decay,⁵ which implies that a T violation occurs somewhere in nature if CPT invariance holds. Since we began the study presented here considerable progress has been made in the experimental determination of phenomenological parameters which characterize the CP violation,⁶⁻⁹ and numerous experiments have been performed to search for T violation in a variety of decays and reactions involving elementary particles and nuclei, besides neutron and ${}^{19}\text{Ne}$ beta decay.¹⁰⁻¹⁶ However, to date there is no definite evidence for T violation in any of the processes examined, and the basic mechanism for CP violation still remains unknown.

II. THEORETICAL BACKGROUND

We consider the beta-decay transition rate $d\lambda$ in the allowed approximation, for the case in which initial and final nuclear spins are equal to one half: $J_i = J_f = 1/2$. This includes neutron and ^{19}Ne decay. Neglecting all momentum-dependent terms in the beta decay interaction, and summing over the final lepton spins which were not experimentally observed, we have¹⁷

$$d\lambda = \frac{g^2}{(2\pi)^5 \hbar^7 c} F(Z,E) p^2 q^2 dp d\Omega_e d\Omega_\nu \times \xi \left\{ 1 + a(\underline{v}/c) \cdot \hat{q} + \frac{\langle J \rangle}{J} \cdot [A(\underline{v}/c) + B\hat{q} + D(\underline{v}/c) \times \hat{q}] \right\} \quad (1)$$

Here $F(Z,E)$ is the Fermi function; p , v , and E are the magnitudes of the momentum, velocity, and energy, respectively, of the electron; $q = c^{-1} (E_{\text{max}} - E)$ is the magnitude of the neutrino momentum and \hat{q} is a unit vector in its direction, and $d\Omega_e$, $d\Omega_\nu$ are differential solid angles for the electron and neutrino, respectively. The spin polarization of the initial nucleus is given by $\langle J \rangle / J$. In the above equation and in the following, the upper sign refers to positron emission, the lower sign to negatron emission.

If final-state electromagnetic interactions are ignored the quantities ξ , A , B , and D are given by

$$\xi = |C_\nu|^2 |\langle 1 \rangle|^2 (1 + |\rho|^2) \quad , \quad (2)$$

$$A = \frac{\pm \frac{2}{3} |\rho|^2 - \frac{2}{\sqrt{3}} |\rho| \cos(\theta + \phi)}{1 + |\rho|^2} \quad , \quad (3)$$

$$B = \frac{\frac{2}{\sqrt{3}}|\rho|^2 - \frac{2}{\sqrt{3}}|\rho|\cos(\theta+\phi)}{1+|\rho|^2}, \quad (4)$$

$$D = \frac{\frac{2}{\sqrt{3}}|\rho|\sin(\theta+\phi)}{1+|\rho|^2} \quad (5)$$

Here $\rho = \frac{C_A \langle \sigma \rangle}{C_V \langle 1 \rangle} = \left| \frac{C_A}{C_V} \right| e^{i\phi} \cdot \left| \frac{\langle \sigma \rangle}{\langle 1 \rangle} \right| e^{i\theta}$, where C_V and C_A are the V, A coupling constants, respectively, and $\langle 1 \rangle$ and $\langle \sigma \rangle$ are the Fermi and Gamow-Teller matrix elements, respectively. Also, θ is the relative phase of $\langle \sigma \rangle$ and $\langle 1 \rangle$, and ϕ is the relative phase of C_A and C_V . If T invariance holds, ρ is real and $\sin(\theta+\phi) = 0$. Thus when Coulomb corrections are ignored as in Eq. 5, $D = 0$. (Actually we shall set $\theta(n) = 0$ and $\theta(^{19}\text{Ne}) = \pi$ in agreement with the usual phase conventions and the nuclear wavefunction¹⁶ of ^{19}Ne , and assume that T violation appears as a departure of $\sin \phi$ from zero.)

The Coulomb correction to D has been calculated to first order in $\alpha Z/p$ by Jackson, Treiman, and Wyld.¹⁷ They find, for $J_i = J_f = 1/2$,

$$D_{\text{Coulomb}}^{(1)} = \left(\frac{2mc}{\sqrt{3}} \right) \left(\frac{\alpha Z}{p} \right) \langle 1 \rangle \langle \sigma \rangle \times \frac{\text{Re}(C_S C_A^* - C_V C_T^* + C_S' C_A'^* - C_V' C_T'^*)}{(|C_S|^2 + |C_V|^2 + |C_S'|^2 + |C_V'|^2) |\langle 1 \rangle|^2 + (|C_T|^2 + |C_A|^2 + |C_T'|^2 + |C_A'|^2) |\langle \sigma \rangle|^2} \quad (6)$$

Here, α is the fine structure constant and m is the electron rest mass. The right hand side of Eq. (6) vanishes for a pure V,A interaction. The upper limits on S and T terms in the beta interaction may be determined from experimental upper limits on the Fierz terms b_F and b_{GT} for Fermi and Gamow-Teller transitions, respectively. These terms are given by¹⁹

$$b_F = \frac{[C_S^* C_V + C_S'^* C_V' + cc]}{(|C_V|^2 + |C_V'|^2 + |C_S|^2 + |C_S'|^2)},$$

$$b_{GT} = \frac{[C_T^* C_A + C_T'^* C_A' + cc]}{(|C_A|^2 + |C_A'|^2 + |C_T|^2 + |C_T'|^2)}.$$

From electron-neutrino angular correlation experiments²⁰⁻²² one knows that $|C_S|^2 \ll |C_V|^2$ and $|C_T|^2 \ll |C_A|^2$. With these results and the substitutions $s = C_S/C_V$, $s' = C_S'/C_V'$, $t = C_T/C_A$, and $t' = C_T'/C_A'$, we obtain

$$b_F \cong \text{Re}(s+s')$$

$$b_{GT} \cong \text{Re}(t+t')$$

Employing these substitutions in Eq. (6), we find

$$D_{\text{Coulomb}}^{(1)} \cong \frac{2}{\sqrt{3}} \frac{\rho}{1+\rho} \frac{(\alpha Z)}{p} (\text{mc}) (b_F + b_{GT})$$

where for this discussion we assume that ρ is real. An upper limit $(b_F) < 0.1$ is obtained by Gerhart²³ from consideration of the constancy of ft values for the pure Fermi $0^+ \rightarrow 0^+$ transitions. Limits of $|b_{GT}| < 0.03$ and $|b_{GT}| < 0.05$ have been found by Sherr and Miller²⁴ and by Leutz and Wenniger,²⁵ respectively, from measurements of the ratio of K capture to positron emission in the $3^+ \rightarrow 2^+$ pure GT transition of ²²Na. Using $b_F < 0.1$ and $b_{GT} < 0.05$, and for ¹⁹Ne, $\langle \frac{\alpha Z}{p} \rangle \text{mc} = \frac{1}{45}$ and $\rho = -1.60$, we find

$$D_{\text{Coulomb}}^{(1)} (^{19}\text{Ne}) \leq 0.0017 \quad (7)$$

Although the second-order Coulomb correction $D_{\text{Coulomb}}^{(2)}$ has not been calculated, it should have order of magnitude

$$D_{\text{Coulomb}}^{(2)} \approx \left(\frac{\alpha t}{p}\right)^2 (\text{mc})^2 \approx 0.001 \quad (8)$$

if there is no fortuitous cancellation for V, A coupling in higher order.

Finally, Callan and Treiman²⁶ have shown that when momentum-transfer-dependent terms in the beta decay amplitude are taken into account (the most important of these is the 'weak magnetism' term, according to the CVC hypothesis) a nonvanishing Coulomb correction to D appears in first order, even for a pure V, A interaction. For ^{19}Ne they obtain the result

$$D_{\text{Weak Magnetism}}^{(1)}(^{19}\text{Ne}) = 0.00026 \quad p/p_{\text{max}} \quad (9)$$

Summarizing the results of Eq. (7) through (9), we may say that the total electromagnetic correction to $D(^{19}\text{Ne})$ is no more than 0.002 at the most. The present experimental uncertainty for $D(^{19}\text{Ne})$ is ± 0.014 , so that electromagnetic corrections to D can safely be ignored.

III. EXPERIMENTAL METHOD

A. Production and Separation of ^{19}Ne

Neon-19 is produced at the Berkeley 88-inch cyclotron in the reaction $^{19}\text{F}(p,n)^{19}\text{Ne}$, by bombardment of SF_6 gas at 3 atmospheres absolute pressure with 15-MeV protons.²⁷ (See Fig. 1.) The proton beam enters the 2-cm-diameter by 20-cm-long target through a 0.18-mm-thick aluminum foil, which is electroplated with nickel to reduce corrosion from

chemically active by-products of bombarded SF_6 . The foil is supported on the evacuated cyclotron side by a water-cooled laminated nickel-copper collimator. Foils usually withstand 60 μA bombardment for 50 to 100 hours.

The SF_6 flows continuously through the target and serves as a carrier to transport the ^{19}Ne to the atomic beam apparatus, which is about 20 meters from the target. Rapid delivery of ^{19}Ne is essential, since the half-life is only 17 sec; a transit time of 5 seconds is typical. SF_6 and by-products of the bombardment are condensed in a liquid nitrogen-cooled trap (LN, in Fig. 1) to separate them from ^{19}Ne . There are two such traps in the system. While one collects SF_6 , the other is being heated to return its contents to the SF_6 supply tank for repeated use.

Very-short-lived radioactive contaminants such as ^{18}Ne decay before reaching the atomic beam apparatus. The only significant contaminant in the bombarded gas with a half-life more than 3 sec is ^{34}Cl , and it is condensed out along with SF_6 .

B. The Atomic Beam Source

The source consists of a copper cavity, cooled to $T \approx 30^\circ \text{K}$, and with a source slit (S_1 in Fig. 1) defined by two stainless steel jaws. Neon-19 atoms effuse from the source slit in the 1S_0 ground state. Temperature T was chosen as low as possible because the decay probability per unit length of ^{19}Ne in the detector region varies as $v^{-1} \propto T^{-1/2}$, and also the effective solid angle at the source subtended by the polarizing system varies at T^{-1} , for a given polarization of atoms entering the detector. Of course, below 20°K , adsorption of neon atoms on the walls of the source cavity would be appreciable.

The source cavity is attached to the bottom of a liquid helium reservoir by means of a stainless steel tube. Neon-19 reaches the source through another stainless tube, and the equilibrium source temperature is determined by the thermal conduction of these tubes. A baffle inside the source cavity prevents fast ^{19}Ne atoms from going directly through the source slit without making several collisions with cold surfaces inside the cavity. Thus thermal equilibrium is achieved between the cavity and particles in the beam, as is demonstrated from observations of the beam-deflection pattern (see next section).

The source-slit jaws are thick compared with their separation; thus the beam is channeled in the forward direction, with a Claussing factor $K^{-1} \approx 15$. The ^{19}Ne atoms that fail to pass through the foreslit (S_2 , Fig. 1) are recirculated through the source as rapidly as possible by a system of three diffusion pumps (see R-1, R-2, R-3 in Fig. 1). The beam intensity with recirculation is 25 times that without recirculation. It was essential to minimize the effective source volume, since most of the recirculation time (≈ 1 sec total) is spent in the region between the 1-inch mercury diffusion pump (R-1) and the source slit. (Mercury was used here because in similar experiments we have observed severe radiation damage of silicone pump fluids.) The pump R-3 is used to compress the exhaust from the pump R-2 rapidly, since R-1 is too slow for this purpose. A titanium sublimation pump in the recirculation loop prevents pressure buildup in the source and possible clogging due to impurities in the SF_6 , such as N_2 or O_2 .

Channeling of the beam in the forward direction enhanced the beam intensity more than it lowered the recirculation gain, because the time

spent in other parts of the recirculation loop was more than a negligible fraction of the time spent in the effective source volume.

C. Deflection and Beam Polarization

A conventional two-pole deflection magnet²⁸ with cylindrical Hyperco pole tips is employed. The length is 100 cm, and the field and gradient are respectively 11 kG and 22 kG/cm at the beam axis. A hexapole deflection magnet was not used because the conductance of the circular source aperture required for such a magnet would be unacceptably small.

Figure 1 indicates schematically how the polarized beam component trajectories and the direction of nuclear polarization along the beam are defined by the magnet and slit system, for the purpose of measuring "D." The source slit and the exit slit are on the center axis of the apparatus and the collimator slit is displaced from the axis by an amount X_C . (Dimensions and positions of the slits as well as estimated beam fluxes are given in Table I.) When $X_C > 0$ (upward from the Z axis in Fig. 1) atoms must be accelerated in the -X direction to pass through all three slits. Thus the selected beam is polarized antiparallel to the magnetic field (the magnetic moment of ^{19}Ne is negative). When $X_C < 0$, as indicated by the dashed trajectory, the polarization is parallel to the field. The deflections are extremely small, so the difference between the paths of the two partial beams through the detector chamber is completely negligible. For the purpose of measuring "D" the spins are turned adiabatically through 90 deg as the atoms emerge from the deflection magnet, and a weak magnetic field is maintained parallel to the beam as it passes through the detector chamber. For measurements of B the magnetic field is kept parallel to the X direction over the entire length of the apparatus.

The final vacuum chamber (Fig. 1) contains the polarization detector, which is used to monitor the beam intensity and polarization. It consists of a hollow cylinder parallel to the X axis with counters adjacent to the thin end walls. Neon-19 beam atoms enter the cylinder through a channel (with dimensions given in Table I) and are stored for about 3 sec; thus many decay there. Actually, only about 10% of the beam arriving in the final chamber traverses the channel. The remainder strikes the solid piece out of which the channel is cut, and is pumped away.

The beam flux through the channel into the polarization detector is shown in Fig. 2a as a function of the displacement X_C of the collimator slit from the beam axis. The solid curves are computed values. The "magnet off" curve is normalized to the experimental points. The "magnet on" curve depends²⁹ on the source temperature, the deflection-magnet length and field gradient, the positions and dimensions of the slits and channel entrance,²⁷ and the magnetic moment of ¹⁹Ne (previously measured). The effective source temperature was determined by measuring the ratio of the beam intensity (deflection magnet on) to the beam intensity (deflection magnet off) (Fig. 2a). The intensities were measured with the polarization detector system with the collimator at $X_C = 0$. With T thus determined, it was possible to calculate the beam intensity and polarization P in the detector chamber as a function of X_C . (Note that $P_A = 1.00$ for atoms going through the channel if $|X_C| > 0.050$ cm, but that $|X_C|$ must be greater than 0.106 cm to give $P = 1.00$ for all beam atoms in the detector chamber (see Fig. 2c). The polarization factor P is defined by

$$P = \frac{F_{+1/2} - F_{-1/2}}{F_{+1/2} + F_{-1/2}},$$

where the factor F is proportional to the number of ^{19}Ne nuclei in state m_J whose decays are observed. If d_m is the probability of observing a decay from state m and ϕ_m is the beam intensity in that state, then $F_m = d_m \phi_m$. It is important to note that in this experiment, $d_{-1/2} \neq d_{+1/2}$ for measurements of D and B . This is because the velocity distribution of beam atoms entering the detector chamber is truncated differently for each m state by the deflection system.

Figure 2c illustrates the calculated intensity and polarization of the beam which passes through the exit slit (S_5) as a function of the collimator position. Our data were collected at $X_C = \pm 0.050$ cm, corresponding to a detector-chamber polarization of $P = 0.87 \pm 0.10$.

D. Detector Arrays

1. Apparatus

The detectors are arranged in two independent and essentially identical banks, each consisting of four positron detectors and four ion detectors in an octagonal array (Fig. 3). The ^{19}Ne beam passes through the center of each array along the Z axis. Observed decays occur in an electric field-free region of length 6 cm for each array, enclosed by the inner octagonal grid at -18 kV. A weak magnetic field is imposed to maintain the beam polarization, but it has a negligible effect on the orbits of all charged decay products. For the measurement of B the beam polarization lies along the X direction in the detector plane. For the D measurement, the beam polarization lies along the beam (Z) axis perpendicular to the detector plane.

Positrons are detected directly with Pilot B plastic scintillators mounted on RCA type 8054 photomultiplier tubes. The maximum positron energy is 2.216 MeV, and our pulse discriminators are set to exclude positrons below 0.62 MeV. (The 0.625-MeV internal conversion line of ^{137}Ba accompanying the decay of ^{137}Cs was used for pulse-height calibration.) The recoil ions $^{19}\text{F}^-$ are emitted at the beam axis and drift a distance of about 5 cm to the -18 kV grid with kinetic energies between 0 and 210 eV. They are then accelerated by the electric field between the inner and outer octagonal grids, the latter being maintained at -9 kV (see Fig. 4). An ion entering any one of the ion detectors then goes on to strike an aluminum secondary emission surface, ejecting six electrons on the average for an ion kinetic energy of 9 keV. The secondary electrons are accelerated to ground potential and crudely focused to a spot about 1 cm in diameter on a Pilot B plastic scintillator of 0.022 cm thickness, which is coated with a grounded thin (100 Å) conducting layer of aluminum. The scintillator is coupled to a short light pipe and thence to a high-gain-low-noise photomultiplier tube (RCA 8575). The ion detectors have an overall efficiency of about 88%, and the pulse-height distribution for ion counts is well separated from photomultiplier noise, as is shown in Fig. 5. Further details on the ion detector are published elsewhere.³⁰

A schematic diagram of the counting electronics is shown in Fig. 6.

2. Method of Collecting Data

Coincidences are recorded for each ion counter with the two electron counters separated from it by a nominal angle of 135 deg (e.g., d-2, a-2 in Fig. 3). There are eight such coincidence pairs for each bank.

It is convenient to classify the coincidence pairs as "regular" pairs and associated "image" pairs as shown in Table II. For the "D" experiment, each "regular" pair, labeled with index $i = 1, \dots, 8$ in Table IIA, would have a greater counting rate than its corresponding "image" for the spin polarization along $+Z$, if $D > 0$ and all pairs had equal efficiencies. Although the efficiencies are in fact unequal, as is shown in Table IIA, every counter belongs to an equal number of "regular" and "image" pairs. Thus instrumental asymmetries arising from differences in detector efficiencies cancel almost exactly, as do many other possible systematic effects, when data are collected in approximately equal amounts for both signs of nuclear polarization.

Let n_i be the total counts (corrected for background) obtained in the D experiment for the i th pair, and let n'_i be that of its image. Coefficient D is obtained from the formula:

$$D = \frac{1}{2PSG_D} (\bar{\Delta}_{DN} + \bar{\Delta}_{DS}) , \quad (10)$$

where S and G_D are a positron backscattering correction and a "geometry" factor respectively, the latter taking into account finite solid angles, spatial extent of the decay region, and momentum distribution of the decay particles. Also, Δ_{DN} and Δ_{DS} are defined by

$$\bar{\Delta}_{DN} = \frac{1}{8} \sum_{i=1}^4 \left[\left(\frac{n_i - n'_i}{n_i + n'_i} \right)_{X_C > 0} - \left(\frac{n_i - n'_i}{n_i + n'_i} \right)_{X_C < 0} \right] , \quad (11)$$

$$\bar{\Delta}_{DS} = \frac{1}{8} \sum_{i=5}^8 \left[\left(\frac{n_i - n'_i}{n_i + n'_i} \right)_{X_C > 0} - \left(\frac{n_i - n'_i}{n_i + n'_i} \right)_{X_C < 0} \right] . \quad (12)$$

Here $X_C > 0$, $X_C < 0$ refer to the collimator position and thus to the sign of nuclear polarization. (Factors S and G_D are discussed in detail in Part IV.)

For the measurement of "B," "regular" and "image" pairs, labeled by index j, are given in Table IIB for the polarization along the +X direction. For each j, the regular count rate exceeds that of its corresponding image if the pairs are equally efficient and $B < 0$. If n_j and n'_j are defined as the total counts after background correction in the jth pair and its corresponding image, respectively, B is given by

$$\frac{1}{2} (\bar{\Delta}_{BN} + \bar{\Delta}_{BS}) = PS(BG_B + AG_{AB}) \quad , \quad (13)$$

$$\frac{1}{2} (\bar{\Delta}_{BN}^* + \bar{\Delta}_{BS}^*) = PS(BG_B^* + AG_{AB}^*) \quad , \quad (14)$$

where

$$\bar{\Delta}_{BN} = \frac{1}{4} \sum_{j=1}^2 \left[\left(\frac{n_j - n'_j}{n_j + n'_j} \right)_{X_C > 0} - \left(\frac{n_j - n'_j}{n_j + n'_j} \right)_{X_C < 0} \right] \quad , \quad (15)$$

$$\bar{\Delta}_{BN}^* = \frac{1}{4} \sum_{j=3}^4 \left[\left(\frac{n_j - n'_j}{n_j + n'_j} \right)_{X_C > 0} - \left(\frac{n_j - n'_j}{n_j + n'_j} \right)_{X_C < 0} \right] \quad , \quad (16)$$

$$\bar{\Delta}_{BS} = \frac{1}{4} \sum_{j=5}^6 \left[\left(\frac{n_j - n'_j}{n_j + n'_j} \right)_{X_C > 0} - \left(\frac{n_j - n'_j}{n_j + n'_j} \right)_{X_C < 0} \right] \quad , \quad (17)$$

$$\bar{\Delta}_{BS}^* = \frac{1}{4} \sum_{j=7}^8 \left[\left(\frac{n_j - n'_j}{n_j + n'_j} \right)_{X_C > 0} - \left(\frac{n_j - n'_j}{n_j + n'_j} \right)_{X_C < 0} \right] \quad . \quad (18)$$

The distinction is made between starred and unstarred terms here because $G_B^* \neq G_B$. Note also that for nuclear polarization along the X direction a small contribution to the observed asymmetry arises from the beta decay asymmetry coefficient A (which is measured independently).

A small misalignment of the polarization axis does not contribute an appreciable false increment to D in spite of the large value of B. (See Appendix A for details.)

Data were collected over many 20-min counting cycles, in which the collimator was first set for 10 min at $X_C = +0.050$ cm and then reset at $X_C = -0.050$ cm for the next 10 min. Thus counts were accumulated for equal intervals at opposite polarizations, $P = 0.87 \pm 0.10$.

3. Background

There were two main sources of background: first, γ radiation from positrons annihilating in the source and to a lesser extent in the gas-handling system; and second, decay of stray ^{19}Ne in the detector region.

The former was measured once every few counting cycles by accumulating coincidences with the collimator deflected far from the center axis and the beam thus completely blocked from the detector chamber.

The latter originated principally from the scattering of the ^{19}Ne beam by residual gas (e.g., N_2 , O_2 , pump oil vapor) in the detector chamber. This part of the stray gas background was proportional to the detector chamber pressure, and was appreciable even at typical operating pressures (1 to 4×10^{-7} Torr). The migration of residual ^{19}Ne from

other chambers into the detector chamber also contributed a small amount to the stray gas background in spite of the provision of a number of stages of differential pumping (see Fig. 1).

The stray gas background was determined from independent measurements of: (a) the fraction f of beam flux which is converted into stray ^{19}Ne by collisions with residual gas, etc; and (b) the relative efficiency ϵ of counter pairs for stray ^{19}Ne decay versus beam ^{19}Ne decay.

A positron counter in the foreline of the detector chamber vacuum system was used to measure f (Fig. 1). With valves V_1 , V_2 , and V_3 closed, all the beam was scattered and collected in the counter. After several half-lives a steady state was achieved and the count rate N_C was measured. With valves V_1 and V_2 open but V_3 closed, only the usual stray ^{19}Ne was collected and the count rate N_0 was measured. The background rate N_B was measured with the beam blocked at the collimator. Thus from the formula

$$f = \frac{N_0 - N_B}{N_C - N_B}$$

we obtain $f \approx 0.05$ to 0.10 , depending on residual gas pressure.

Quantity ϵ was determined from the total coincidence count rates in all pairs with valves V_1 and V_2 open (C_0) and with valves V_1 and V_2 closed (C_C):

$$\epsilon = \frac{C_C - C_0}{C_0 - fC_C}$$

We obtained $\epsilon \approx 4$. Thus the total scattered gas background was 20% to 40%, depending on f . The value of ϵ is in reasonable agreement with an estimate based on the measured pumping speed of the detector vacuum system.

Electric sparks and field emission from the -9- and -18-kV electrodes caused us much difficulty, contributing to the singles background in ion counters, and thus to the accidental coincidence rate. It was necessary to polish all electrode surfaces, guard electrostatically all standoff insulators and high-voltage feedthroughs, maximize spacings of electrodes, and take scrupulous care to prevent dust from entering the chamber when it was open to atmosphere. Finally it was necessary to "clean" surfaces by applying abnormally high electrode voltages for several hours prior to each run. Nevertheless, many hours of running time were lost with electrical noise problems, the worst being intermittent sparking between the ion phototube shields and the outer (-9-kV grid shield (see point P in Fig. 4).

4. Time-of-Flight Spectrum

Because the $^{19}\text{F}^-$ ions have less than 210 eV kinetic energy, and must drift from the beam axis to the inner octagonal grid before acceleration, the e^+ , $^{19}\text{F}^-$ coincidences are delayed by 1.75 μsec or more. The observed positron-recoil ion delay spectrum is shown in Fig. 7. Note that the large background of coincidences with short delay is primarily from scattered gas. The solid curve in Fig. 7 was calculated from the decay kinematics and the detector array geometry. The agreement between experiment and calculation is very satisfactory.

5. Polarization Detector

The polarization detector consists of a hollow aluminum cylinder parallel to the X axis, with height 2 cm and inner diameter 12 cm (Fig. 1). The end walls are 0.005-cm-thick Mylar sheet, through which positrons pass with very small energy loss. Neon-19 atoms entering the cylinder

are stored there about 3 sec, during which time they each make about 10^4 wall collisions. In spite of this long time, nuclear polarization is preserved, with direction defined by a reasonably homogeneous magnetic field $H_D = 65$ gauss parallel to the cylinder axis. From the storage time, the calculated solid angle subtended by each positron counter, and the known discriminator bias on each counter, the sum of counting rates $\frac{dN_1}{dt} + \frac{dN_2}{dt}$ in the two positron counters is computed to be

$$\frac{dN_1}{dt} + \frac{dN_2}{dt} = 0.062 F_9 \quad ,$$

where F_9 is the ^{19}Ne flux through the channel. This sum is used to monitor the beam intensity. The asymmetry A is determined from

$$A = \frac{1}{P_A S_A G_A \langle \frac{v}{c} \rangle} \Delta_A \quad , \quad (19)$$

where:

$$\Delta_A = \frac{1}{2} \left[\left(\frac{N_1 - N_2}{N_1 + N_2} \right)_{X_C > 0} - \left(\frac{N_1 - N_2}{N_1 + N_2} \right)_{X_C < 0} \right] \quad , \quad (20)$$

and P_A , S_A , and G_A are the fractional polarization, backscattering correction, and geometry factor, respectively, all referred to the polarization detector.

The factor $G_A \approx 0.62$ is determined by numerical integration. The factor $S_A = 0.92$ is calculated by using methods similar to those employed for the calculation of S (see Sec. IV-D).

The polarization of entering ^{19}Ne is known from beam deflection measurements and calculations to be 100% at $X_C = \pm 0.050$ cm. When the polarization detector cylinder storage time is varied (by using different channel lengths) no variation in Δ and thus no evidence for spin relaxation is found at $H_D = 65$ gauss. Relaxation effects, however, reduce the polarization to 80% at $H_D = 20$ gauss and to 35% at $H_D = 10$ gauss. In a similar experiment on ^{23}Ne , the relaxation time was observed to depend on H_D as $T \approx H_D^4$. Thus at 65 gauss, we estimate a depolarization correction of 0.4%. The relaxation mechanism is thought to be nonadiabatic transitions during wall collisions arising from inhomogeneities in H_D , rather than short-range dipole fields at the walls. No special treatment of the bulb walls is needed to prevent relaxation. The positron back-scattering correction is smaller than in previous experiments because the cylinder and detectors are now made with low-Z materials.

IV. DATA, CORRECTIONS, AND RESULTS

A. D Data

Data for the measurement of D were accumulated over six runs, each lasting about 50 hours. The data are summarized in Table III. As noted in Sec. III-D2, quantity D is obtained from the background-corrected coincidence counts by means of Eqs. (10), (11), and (12) (see also Table IIa). The factors P , S , and G_D have these values: $P = 0.87 \pm 0.10$ (see Sec. III-B); $S = 0.80 \pm 0.05$ (see Sec. IV-D below), $G_D = 0.75 \pm 0.02$ (see Sec. IV-E below). The final result is

$$D = 0.002 \pm 0.014, \quad (21)$$

where the uncertainty is purely statistical (standard deviation).

During the first D run the true coincidence rate was about 0.2 counts/min per counter pair. Improvements in the recirculation system and source raised this figure to about 0.5 c/min per counter pair by the sixth run. Neon-19 beam fluxes given in Table I are based on count rates observed in the polarization detector with this improved beam. A computation of the coincidence count rate based on the flux through slit S_5 (Fig. 1) is in good agreement with the observed rate.

B. B Data

Table IV summarizes the data for B, which is obtained from the background-corrected coincidence counts, using Eqs. (13) through (18) (see also Table IIb). Factors P and S are the same as in the previous section. Also,

$$\begin{aligned} G_B &= +0.59, & G_B^* &= +0.57, \\ G_{AB} &= +0.60, & G_{AB}^* &= +0.70 . \end{aligned}$$

When these results are combined with the experimental value $A = -0.039 \pm 0.002$ (see Sec. IV-C below), the final result for B is

$$B = -0.90 \pm 0.13 . \quad (22)$$

This value of B is not unexpected, inasmuch as it merely confirms what we already know about the coupling constants and matrix elements [see Eq. (4)]. Our observations of B were useful because they demonstrated that the apparatus functioned properly. The uncertainty in B is almost wholly due to the uncertainties in P, S, and G and hardly at all due to statistics.

C. A Data

Data for A are summarized in Table V. They were accumulated at the same time as the 'D' data. The polarization of run 1 is lower than that of subsequent runs because thermal equilibrium was not completely achieved between beam particles and the source in the first run. Only runs 2 through 6 are averaged to compute Δ_A . Using Eqs. (19) and (20) and the values

$$G_A = 0.62 \pm 0.01 ,$$

$$S_A = 0.92 \pm 0.05 ,$$

$$P_A = 1.00 ,$$

and

$$\left\langle \frac{V}{C} \right\rangle = 0.947 ,$$

we find

$$A = -0.039 \pm 0.002 , \quad (23)$$

where the main source of uncertainty is S_A .

D. Positron Backscattering Correction

Most of the positrons emitted during decays in flight through the detector chamber do not strike the desired positron counter, but instead strike some other part of the detector array. Some of these positrons may backscatter into the positron counter and register spurious counts. If b is the number of such backscattered counts and n is the number of true counts, then the observed number is

$$n_1 = n + b .$$

Because of the symmetry of the detector bank, and since the positrons are emitted very nearly isotropically from polarized ^{19}Ne nuclei, we assume b is the same for all counter pairs. Then

$$\frac{n_1 - n'_1}{n_1 + n'_1} = \frac{n - n'}{n + n' + 2b} \approx \frac{n - n'}{n - n'} \left(1 - \frac{b}{n}\right)$$

for $n \approx n'$. Therefore, the backscattering correction factor S is

$$S = 1 - b/n .$$

Factor b/n was calculated from the known geometry using the fact that $\approx 20\%$ of positrons in this energy range backscatter when striking thick aluminum. In estimating S it was assumed that all positrons that backscatter into the positron detectors are actually counted. This is probably not so, because the energy spectrum of backscattered positrons is unknown, and almost certainly there is considerable energy loss on backscattering. Therefore, our computed values of S probably represent a lower limit.

E. Geometry Correction Factors

We transform the differential transition rate $d\lambda$ of Eq. (1) by eliminating neutrino variables q , $d\Omega_\nu$, and introducing the recoil ion momentum \underline{r} and the ion differential solid angle $d\Omega_r$. Note that the kinetic energy of a ^{19}Ne beam atom is less than 0.0025 eV, so that the equation

$$\underline{p} + \underline{q} + \underline{r} = 0$$

is satisfied to a very good approximation in the laboratory frame.

Thus writing

$$r = |r| = -p\hat{p}\cdot\hat{r} \pm \{q^2 - p^2 [1 - (\hat{p}\cdot\hat{r})^2]\}^{1/2}$$

we find

$$d\lambda \propto \left[\frac{pF(Z,E)}{E} \right] E^2 (E_0 - E)^2 dE d\Omega_e d\Omega_r \frac{r}{q} \cdot \left| \frac{-p\hat{p}\cdot\hat{r}}{\{q^2 - p^2 [1 - (\hat{p}\cdot\hat{r})^2]\}^{1/2}} \pm 1 \right| \\ \times \left[1 - \frac{ap}{qE} (r\hat{p}\cdot\hat{r} + p) + \frac{Ap}{E} (\hat{J}\cdot\hat{p}) - \frac{B}{q} (r\hat{J}\cdot\hat{r} + p\hat{J}\cdot\hat{p}) - \frac{Dp}{qE} \hat{J}\cdot(\hat{p}\times\hat{r}) \right] \quad (24)$$

The two signs in Eq. (24) are necessary, since for $p > q$, and for fixed angle between \hat{p} and \hat{r} , there are two possible neutrino momenta q which satisfy the condition $\underline{p} + \underline{q} + \underline{r} = 0$. Thus for $p > q$ the total rate is the sum of the rate with the (+) sign and that with the (-) sign;³¹ for $p < q$ only the (+) sign applies. In evaluating the RHS of Eq. (24) the factor $p F/E$ is obtained from standard tables.

In Eq. (24) it is clear that for the "D" magnetic field configuration, the A and B terms average to zero for regular and image pairs. Also, the D term contributes to the difference ($n-n'$), while the unity and "a" terms contribute to ($n+n'$). The geometry factor G_D is defined as the average of the D term divided by the average value of the sum of the unity and "a" terms. Actually, $a = 0.0413 \pm 0.0034$ is negligible, and it is ignored. The averages were computed over all accepted angles between \hat{I} , \hat{p} , and \hat{r} , over all accepted beta energies ($T_{\min} = 0.625$ MeV to $T_{\max} = 2.216$ MeV), and over the accepted ion-recoil time-delay interval (1.75 to 3.25 μ sec). Each counter is assumed to be uniform in efficiency over its acceptance aperture. This was in fact verified for both ion counters³⁰ and positron counters. Note that the transition rate contains a factor which is singular when $\hat{p}\cdot\hat{r} = 0$, so due care must be exercised

in the computations. The result is

$$G_D = 0.75 \pm 0.02 ,$$

where the uncertainty arises from numerical approximations.

The other geometry factors are evaluated in similar fashion. With the magnetic field in the "B" configuration, only the "D" term in $d\lambda$ averages to zero. The A and B terms both differ in sign for regular and image pairs, so these terms contribute to $(n-n')$ but not to $(n+n')$, which are, as before, proportional to the sum of unity and "a" terms. Thus G_B is the computed average of the "B" term divided by the average of the sum of unity and "a" terms. The calculated values are

$$G_B = 0.59 , \quad G_B^* = 0.57 ,$$

$$G_{AB} = -0.60 , \quad G_{AB}^* = -0.70 .$$

All computations were carried out on the CDC 6600 computer.

V. CONCLUSIONS

We now present a comparison of our experimental results with those obtained from observations of the decay of polarized neutrons.

A. Neutron Measurements

For neutron decay, the measured values of A, B, and D, are

$$A(n) = -0.11 \pm 0.02 \quad (\text{Ref. 2}) ,$$

$$B(n) = +0.88 \pm 0.15 \quad (\text{Ref. 2}) ,$$

$$D(n) = +0.01 \pm 0.01 \quad (\text{Ref. 4}) .$$

The quantity $\rho(n)$ is obtained from the neutron ft value through the formula

$$(ft)^{-1} = \frac{(\hbar c)^5}{2\pi^3 \hbar^2 \hbar^7 c} G^2 |C_V|^2 |\langle 1 \rangle|^2 [1 + |\rho|^2] .$$

Using the value $G = 1.4034 \pm 0.0016 \times 10^{-49}$ erg cm³ as obtained from the $O^+ \rightarrow O^+$ pure Fermi transitions³² and taking $C_V = \langle 1 \rangle = 1$ and the latest value of the neutron half-life,³³ we obtain

$$|\rho(n)| = 2.13 .$$

Thus, from Eq. (5), taking $\theta(n) = 0$, we find

$$D(n) = -0.443 \sin \phi .$$

Now $\cos \phi < 0$ for neutron decay, since

$$A(n) + B(n) = -\frac{4}{\sqrt{3}} \frac{|\rho| \cos \phi}{1 + |\rho|^2} \approx +0.8 .$$

Therefore

$$\phi(n) = 178.7 \pm 1.3 \text{ deg} ,$$

consistent with T invariance.

B. Neon-19 Measurements

The results of this experiment are

$$A(^{19}\text{Ne}) = -0.039 \pm 0.002 , \quad (23)$$

$$B(^{19}\text{Ne}) = -0.90 \pm 0.13 , \quad (22)$$

$$D(^{19}\text{Ne}) = +0.002 \pm 0.014 , \quad (21)$$

We again obtain $|\rho|$ from the ft value. Assuming $\langle 1 \rangle = 1$, since the ^{19}Ne decay is a mirror transition, and taking $ft = 1750 \pm 9$ sec as determined from

$$t_{1/2}(^{19}\text{Ne}) = 17.36 \pm 0.06 \text{ sec} ,$$

and

$$E_{\text{max}}(^{19}\text{Ne}) = 2.216 \pm 0.001 \text{ MeV} ,$$

we find³⁴

$$|\rho(^{19}\text{Ne})| = 1.603 \pm 0.006 . \quad (25)$$

Then taking $\theta(^{19}\text{Ne}) = \pi$, we find, from Eq. (5),

$$D(^{19}\text{Ne}) = +0.507 \sin \phi .$$

Again $\cos \phi < 0$, since

$$A(^{19}\text{Ne}) + B(^{19}\text{Ne}) = \frac{4}{\sqrt{3}} \frac{|\rho| \cos \phi}{1 + |\rho|^2} \approx -0.8 .$$

Thus we finally obtain

$$\phi(^{19}\text{Ne}) = 180.2 \pm 1.6 \text{ deg} ,$$

consistent with T invariance and the neutron result.

A value of $|\rho(^{19}\text{Ne})|$ may also be derived from $A(^{19}\text{Ne})$ if we assume $\cos \phi \approx -1$. Thus we obtain,³⁵ from Eqs. (3) and (23),

$$|\rho(^{19}\text{Ne})| = 1.60 \pm 0.01 ,$$

consistent with Eq. (25).

ACKNOWLEDGMENTS

We are pleased to acknowledge the encouragement and support we have received, particularly from Dr. Bernard Harvey, Professor Emilio Segrè, Professor Howard Shugart, and Professor Robert L. Thornton. We also thank Professor Samuel Treiman and Professor Curtis Callan for their clarification of the role of final-state interactions. Finally, we are very grateful to the staff of the 88-inch Cyclotron and to Douglas MacDonald, Donald Landis, Donald Lundgren, John Meneghetti and many others for their excellent technical support.

APPENDIX

Elimination of Systematic Errors in D Due to Magnetic Field Misalignment
in the Detector Chamber. Efficiency Difference Between Coincidence Pairs

We give a simplified calculation to show how the data are combined to minimize a possible systematic error in D, which might be thought to arise from a magnetic field misalignment, owing to the large coefficient B. Suppose that the detectors 1-4, a-e are oriented as shown in Fig. 5 (XY plane), and assume that the magnetic field and spin have direction

$$\hat{I} = \cos \alpha \hat{k} + \sin \alpha \hat{j} .$$

For the purposes of this simple estimate, let the detectors subtend zero solid angle and be located at 0, 45, 90, 135, ... deg with respect to the vertical. Consider decays in which e^+ and ν are emitted at 90 deg relative to each other and $^{19}\text{F}^-$ ion is emitted at 135 deg relative to both. If the nuclear spin polarization is 100%, one can show that the following expressions for the coincidence count rates hold:

$$W_{d2} = K \epsilon_{d2} (1 + b + d) ,$$

$$W_{a2} = K \epsilon_{a2} (1 + b - d) ,$$

$$W_{a1} = K \epsilon_{a1} (1 - b + d) ,$$

$$W_{b1} = K \epsilon_{b1} (1 + b - d) ,$$

$$W_{b4} = K \epsilon_{b4} (1 - b + d) ,$$

$$W_{c4} = K \epsilon_{c4} (1 - b - d) ,$$

$$W_{c3} = K \epsilon_{c3} (1 + b + d) ,$$

$$W_{d3} = K \epsilon_{d3} (1 - b - d) .$$

Here K is a common constant, and the ϵ 's are coincidence-pair efficiencies,

$b = \frac{B \sin \alpha}{\sqrt{2}}$ and $d = D \frac{V}{C} \cos \alpha$. We define

$$4R_D = \frac{W_{2d} - W_{2a}}{W_{2d} + W_{2a}} + \frac{W_{1a} - W_{1b}}{W_{1a} + W_{1b}} + \frac{W_{4b} - W_{4c}}{W_{4b} + W_{4c}} + \frac{W_{3c} - W_{3d}}{W_{3c} + W_{3d}}$$

Now, writing

$$x_1 = \frac{\epsilon_{1a} - \epsilon_{1b}}{\epsilon_{1a} + \epsilon_{1b}}, \quad x_2 = \frac{\epsilon_{2d} - \epsilon_{2a}}{\epsilon_{2d} + \epsilon_{2a}}, \quad x_3 = \frac{\epsilon_{3c} - \epsilon_{3d}}{\epsilon_{3c} + \epsilon_{3d}}, \quad x_4 = \frac{\epsilon_{4b} - \epsilon_{4c}}{\epsilon_{4b} + \epsilon_{4c}},$$

we obtain

$$4R_D = \frac{x_2(1+b)+d}{(1+b)+x_2d} + \frac{x_1-(b-d)}{1-x_1(b-d)} + \frac{x_4(1-b)+d}{(1-b)+x_4d} + \frac{x_3+(b+d)}{1+x_3(b+d)} \quad (A1)$$

If all detector pairs were equally efficient we would have $x_1 = x_2 = x_3 = x_4 = 0$ and thus, for small angles α ,

$$4R_D = 2d + \frac{d}{1+b} + \frac{d}{1-b} \approx 4d \left(1 + \frac{b^2}{2}\right)$$

Taking $B = -1$ and $\alpha = 5$ deg, we find $\frac{b^2}{2} = \frac{1}{4} \sin^2(5 \text{ deg}) \approx 2 \times 10^{-3}$.

This correction is quite negligible at our level of accuracy. Now in fact, the x 's are nonzero, owing to differences in detector-pair efficiencies.

For the north bank of detectors, for example,

$$x_1 = 0.067,$$

$$x_2 = 0.136,$$

$$x_3 = -0.068,$$

$$x_4 = -0.052.$$

However, this does not alter the conclusion that the correction, as obtained from formula (A1) is negligible.

FOOTNOTES AND REFERENCES

- * Work supported by the U. S. Atomic Energy Commission.
- † Present Address: Bell Telephone Laboratories, Murray Hill, New Jersey.
- ‡ Present Address: A.E.R.E. Harwell, Didcot, Berkshire, England.
- ‡ Present Address: Department of Physics, Beloit College, Beloit, Wisconsin.
- ¹ For a preliminary report of the work presented here, see F. P. Calaprice, E. D. Commins, H. M. Gibbs, G. L. Wick, and D. A. Dobson, Phys. Rev. Letters 18, 918 (1967); G. L. Wick, Ph.D. Thesis, Lawrence Radiation Laboratory Report UCRL-17708, July 1967.
- ² M. T. Burgy, V. E. Krohn, T. B. Novey, G. R. Ringo, and V. L. Telegdi, Phys. Rev. 120, 1829 (1960).
- ³ M. A. Clark, J. M. Robson, and R. Nathans, Phys. Rev. Letters 1, 100 (1958).
- ⁴ B. G. Erokolimsky, L. N. Bondarenko, Yu. A. Mostovoy, B. A. Obinyakov, V. P. Zacharova, and V. A. Titov, Phys. Letters 27B, 557 (1968).
- ⁵ J. H. Christenson, J. W. Cronin, V. L. Fitch, and R. Turlay, Phys. Rev. Letters 13, 138 (1964).
- ⁶ T. T. Wu and C. N. Yang, Phys. Rev. Letters 13, 380 (1964).
- ⁷ M. Banner, J. W. Cronin, J. K. Liu, and J. E. Pilcher, Phys. Rev. Letters 21, 1107 (1968).
- ⁸ A. Böhm, P. Darriulat, C. Grosso, V. Kaftanov, K. Kleinknecht, H. L. Lynch, C. Rubbia, H. Ticho, and K. Tittel, Phys. Letters 27B, 321 (1968).
- ⁹ S. Bennett, D. Nygren, H. Saal, J. Steinberger, and J. Sunderland, Phys. Rev. Letters 19, 993 and 997 (1967).
- ¹⁰ W. von Witsch, A. Richter, and P. von Brentano, Phys. Rev. Letters 19, 524 (1967).
- ¹¹ O. C. Kistner, Phys. Rev. Letters 19, 872 (1967).

- ¹²P. D. Miller, W. B. Dress, J. K. Baird, and N. F. Ramsey, Phys. Rev. Letters 19, 381 (1967).
- ¹³C. G. Shull and R. Nathans, Phys. Rev. Letters 19, 384 (1967).
- ¹⁴T. S. Stein, J. P. Carrico, E. Lipworth, and M. C. Weisskopf, Phys. Rev. Letters 19, 741 (1967); Errata, Phys. Rev. Letters 19, 1000 (1967).
- ¹⁵O. E. Overseth and R. F. Roth, Phys. Rev. Letters 19, 391 (1967).
- ¹⁶K. K. Young, M. J. Longo, and J. A. Helland, Phys. Rev. Letters 18, 806 (1967).
- ¹⁷J. D. Jackson, S. B. Treiman, and H. W. Wyld, Jr., Nucl. Phys. 4, 206 (1957). Equations 2-5 in the text can be obtained from the equations of this reference by assuming the usual V,A interaction.
- ¹⁸E. D. Commins and D. A. Dobson, Phys. Rev. Letters 10, 347 (1963).
- ¹⁹See for example, E. J. Konopinski, The Theory of Beta Radioactivity (Clarendon Press, Oxford, 1966), pp. 270, 271, Eqs. (10.12), (10.13).
- ²⁰Ibid., p. 270.
- ²¹J. S. Allen, R. L. Burman, W. B. Hermannsfeldt, P. Stähelin, and T. H. Braid, Phys. Rev. 116, 134 (1959).
- ²²C. H. Johnson, F. Pleasanton, and T. A. Carlson, Phys. Rev. 132, 1149 (1963).
- ²³J. B. Gerhart, Phys. Rev. 109, 897 (1958).
- ²⁴R. Sherr and R. H. Miller, Phys. Rev. 93, 1076 (1954).
- ²⁵H. Leutz and H. Wenninger, Nucl. Phys. A99, 55 (1967).
- ²⁶C. G. Callan, Jr., and S. Treiman, Phys. Rev. 162, 1494 (1967).
- ²⁷D. A. Dobson, Ph.D. Thesis, Lawrence Radiation Laboratory Report UCRL-11169, December 1963.
- ²⁸See for example, N. F. Ramsey, Molecular Beams (Clarendon Press, Oxford, England, 1956), p. 397.
- ²⁹Ibid., p. 89.

³⁰H. M. Gibbs and E. D. Commins, Rev. Sci. Inst. 37, 1385 (1966).

³¹O. Koefoed-Hansen, Kgl. Danske Videnskab. Selskab, Mat.-Fys. Medd. 28, No. 9 (1954), p. 3.

³²J. M. Freeman, J. G. Jenkins, D. C. Robinson, G. Murray, W. E. Burcham, Phys. Letters 27B, 156 (1968).

³³C. J. Christensen, A. Nielsen, A. Bahnsen, W. K. Brown, B. M. Rustad, Phys. Letters 26B, 11 (1967).

³⁴F. P. Calaprice, Ph.D. Thesis, Lawrence Radiation Laboratory Report UCRL-17551, May 1967.

³⁵Reference 1 gives $A(^{19}\text{Ne}) = -0.033 \pm 0.002$. Our present value differs from this because of refinements in data analysis. Reference 27 quotes an incorrect value $|\rho| = 1.68 \pm 0.01$.

Table I. Beam slit positions and dimensions. Beam fluxes.

	Source slit (S ₁)	Collimator ^a slit (S ₃)	Exit slit ^a (S ₅)	Channel ^a (S ₉)
Width (cm)	0.076	0.076	0.25	0.064
Height (cm)	1.25	1.00	0.64	1.00
Thickness (cm)	0.32	----	----	3.18
Distance from source slit (cm)	0	65	188	374
Solid angle of beam (sr)	0.8	1.8×10^{-5}	4.5×10^{-6}	4.0×10^{-7}
Flux of ¹⁹ Ne (atoms/sec)	3×10^{11}	1.7×10^6	4.2×10^5	1.4×10^5

^aBeam fluxes through the (S₃), (S₅), and (S₉) slits are given for the collimator slit at X_C=0 and with the deflection magnet off. Fluxes are based on the measured counting rate in the polarization detector. See Fig. 1 for identification of the slits.

Table II. Counter pairs and efficiencies.

A. Coincidence pairs for "D" experiment

	i	"Regular" pair	Measured relative efficiencies (d-2, e-5 \equiv 1.0)	"Image" pair	Measured relative efficiencies (d-2, e-5 \equiv 1.0)
	1	d-2	1.0	a-2	0.76
North bank	2	b-4	0.83	c-4	0.93
	3	c-3	0.73	d-3	0.84
	4	a-1	0.73	b-1	0.64
	5	h-6	0.85	e-6	0.59
South bank	6	f-8	0.66	g-8	0.78
	7	g-7	0.88	h-7	0.92
	8	e-5	1.0	f-5	0.94

B. Coincidence pairs for "B" experiment

j	"Regular" pair	"Image" pair
1	d-2	a-2
2	c-4	b-4
3	b-1*	c-3*
4	a-1*	d-3*
5	h-6	e-6
6	g-8	f-8
7	f-5*	g-7*
8	e-5*	h-7*

Table III. Compilation of D data.

Magnetic field directions					
Run no.	Deflection field	Axial field in coinc. detector chamber	Direction of spin polarization for $X(C) > 0$	No. of coinc. counts (corrected)	D
1	+ \hat{X}	- \hat{Z}	+ \hat{Z}	3059	+ 0.038 \pm 0.035
2	+ \hat{X}	+ \hat{Z}	- \hat{Z}	5980	+ 0.012 \pm 0.037
3	- \hat{X}	+ \hat{Z}	- \hat{Z}	5563	- 0.022 \pm 0.028
4	- \hat{X}	- \hat{Z}	+ \hat{Z}	3355	- 0.007 \pm 0.047
5	- \hat{X}	+ \hat{Z}	- \hat{Z}	5281	+ 0.010 \pm 0.031
6	+ \hat{X}	- \hat{Z}	+ \hat{Z}	6889	- 0.024 \pm 0.049

Total counts (corrected) 30127

Weighted average D = + 0.002 \pm 0.014

Table IV. Compilation of Δ_B data.

Run	Even pairs		Odd (asterisked) pairs	
	No. of coinc. counts	Δ_B	No. of coinc. counts	Δ_B^*
1	350	0.291 \pm 0.054	417	0.386 \pm 0.045
2	739	0.316 \pm 0.037	680	0.353 \pm 0.038
3	287	0.358 \pm 0.059	270	0.287 \pm 0.061
4	323	0.344 \pm 0.056	327	0.361 \pm 0.055
5	328	0.398 \pm 0.055	347	0.382 \pm 0.054
6	1028	0.348 \pm 0.031	1096	0.389 \pm 0.030
Sum	3055		3137	
Weighted average ($\bar{\Delta}$)		0.340 \pm 0.018		0.366 \pm 0.018

Table V. Compilation of Δ_A data.

Run	Total counts	Δ_A
1	959,123	-0.0168 ±0.00180
2	1,184,247	-0.02121 ±0.00097
3	1,451,344	-0.02107 ±0.00085
4	1,264,922	-0.02248 ±0.00093
5	2,081,788	-0.02159 ±0.00072
6	1,857,914	-0.02019 ±0.00075
Sum	8,799,338	
Weighted average (Runs 2-6) ($\bar{\Delta}_A$)		-0.02131 ±0.0005

FIGURE CAPTIONS

Fig. 1. Schematic diagram of ^{19}Ne atomic beam apparatus. Neon-19 is produced by proton bombardment of SF_6 gas in target. Atomic beam of ^{19}Ne in $^1\text{S}_0$ state emerges from source slit S_1 at 30°K and is polarized by deflection magnet with beam-defining slits S_1 , S_3 , S_5 and channel entrance S_9 . Other slits S_2 , S_4 , S_6 , S_7 , S_8 do not define beam but are used for differential pumping. Polarized beam deflections are grossly exaggerated for pictorial clarity; actual difference of paths between $m_J = \pm 1/2$ beam components is negligible in detector chamber. Measurements of B and D are made from decays in flight in north and south banks; A is determined from decays in polarization detector. Distances l_3 , l_5 , l_9 are referred to in Table I. Stray gas counter is referred to in Sec. III-D3.

Fig. 2. (a) Beam intensity and polarization in polarization detector vs collimator slit position. The solid curves are calculated. The deflected beam profile and the polarization are calculated by using the measured moment [$\mu(^{19}\text{Ne}) = -1.887 \mu_N$] and assuming a source temperature of 30°K and deflection magnet gradient of 22 kG/cm , together with the parameters of Table I. The polarization is 100% for $X_C \geq 0.05\text{ cm}$, which is the optimum operating position. (b) Calculation of source temperature vs ratio of deflected to undeflected intensities through channel. The intensities are measured with the collimator slit (S_3) at $X_C=0$. Operating temperature of source is seen to be about 30°K . (c) Calculation of intensity and polarization of beam which passes through exit slit (S_5) and is observed by detector banks within detector chamber (see Fig. 1) vs collimator slit position. Low count rates prohibited comparison of computed beam profile with measured one.

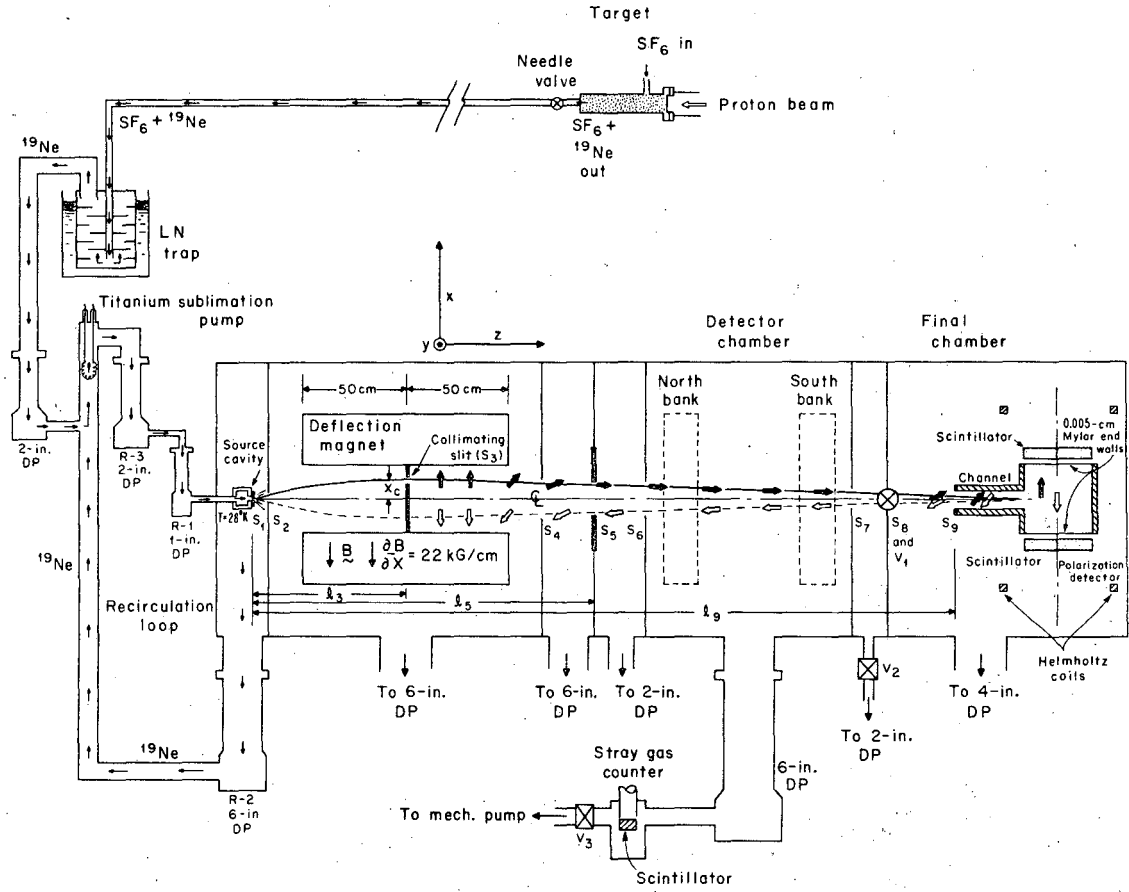
Fig. 3. Cross-sectional view of north detector bank, to scale. The ^{19}Ne atomic beam travels out of the page. A typical coincidence (d-2) is shown. The south detector is essentially identical. Insert in figure shows labeling of counters for south bank.

Fig. 4. Detector array. For clarity only one ion detector and one positron detector are shown in the figure. The particle trajectories from a typical decay event are shown.

Fig. 5. Pulse-height calibration curve for one of the ion detectors. The detectors were calibrated with 9-keV K^+ ions produced by inserting a hot tungsten filament coated with KHF_2 into the detector array along the beam axis and grounding the inner shield. The response of our detectors to K^+ ions and F^- ions is compared in Ref. 30.

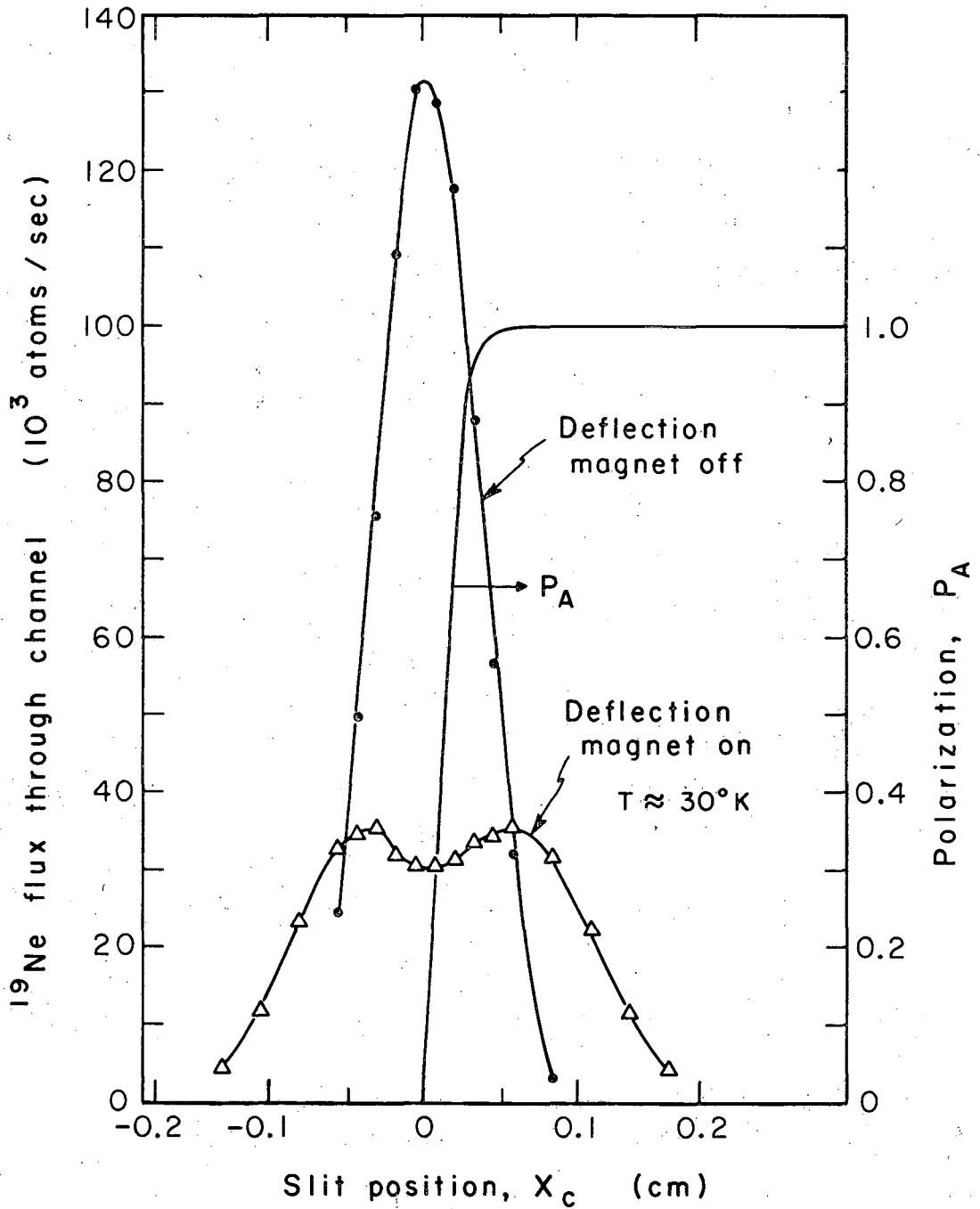
Fig. 6. Schematic diagram of the counting electronics. The delay and the gate on the positron pulse are set for 1.75 to 3.25 μsec . The interface unit routes all singles and coincidences to specific channels in the pulse-height analyzer, which is used to scale all singles and coincidences in each collimator position.

Fig. 7. Positron-recoil-ion coincidence counts vs delay time, as obtained with four coincidence pairs. The solid curve is computed from the theoretical ion energy distribution, and includes a contribution from two sources of background. The triangular data points indicate the measured accidental coincidence counts which arise from the uncorrelated singles background in each detector of the coincidence pair. The dashed curve indicates the additional background contribution, measured separately, due to the decay of residual ^{19}Ne gas in the detector region. The solid points are measurements of the counts with the ^{19}Ne beam in addition to these sources of background. Coincidences in the range 1.75 to 3.25 μsec were accepted to determine B and D.



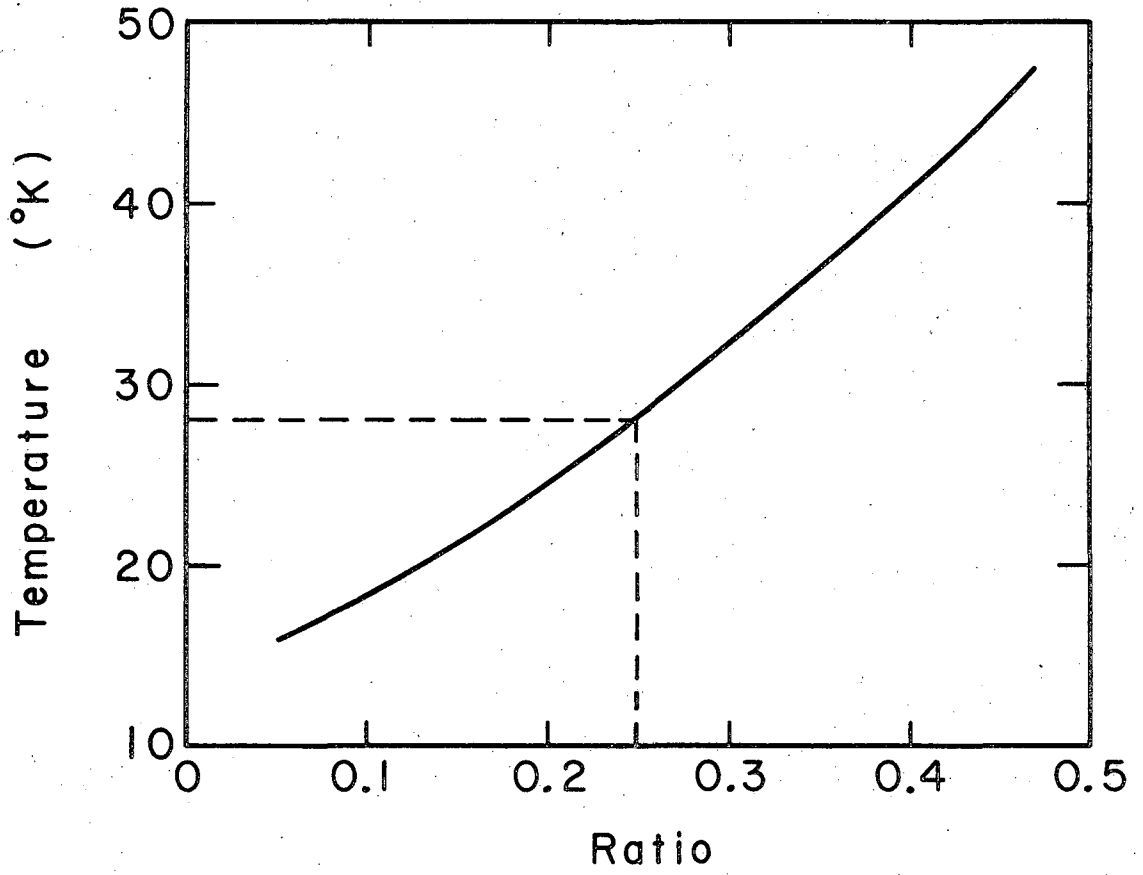
XBL69I-1627

Fig. 1



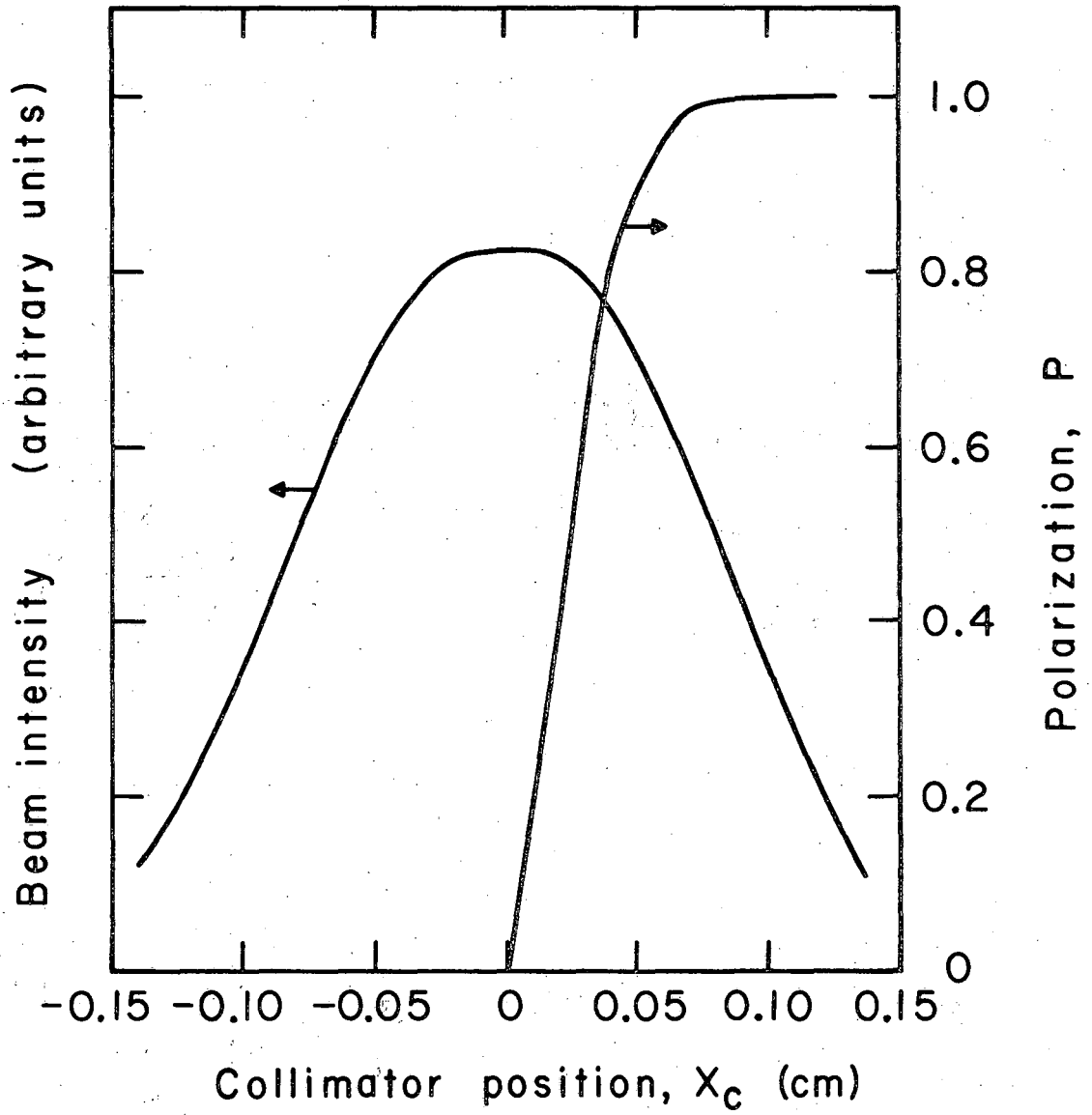
XBL691-1629

Fig. 2a



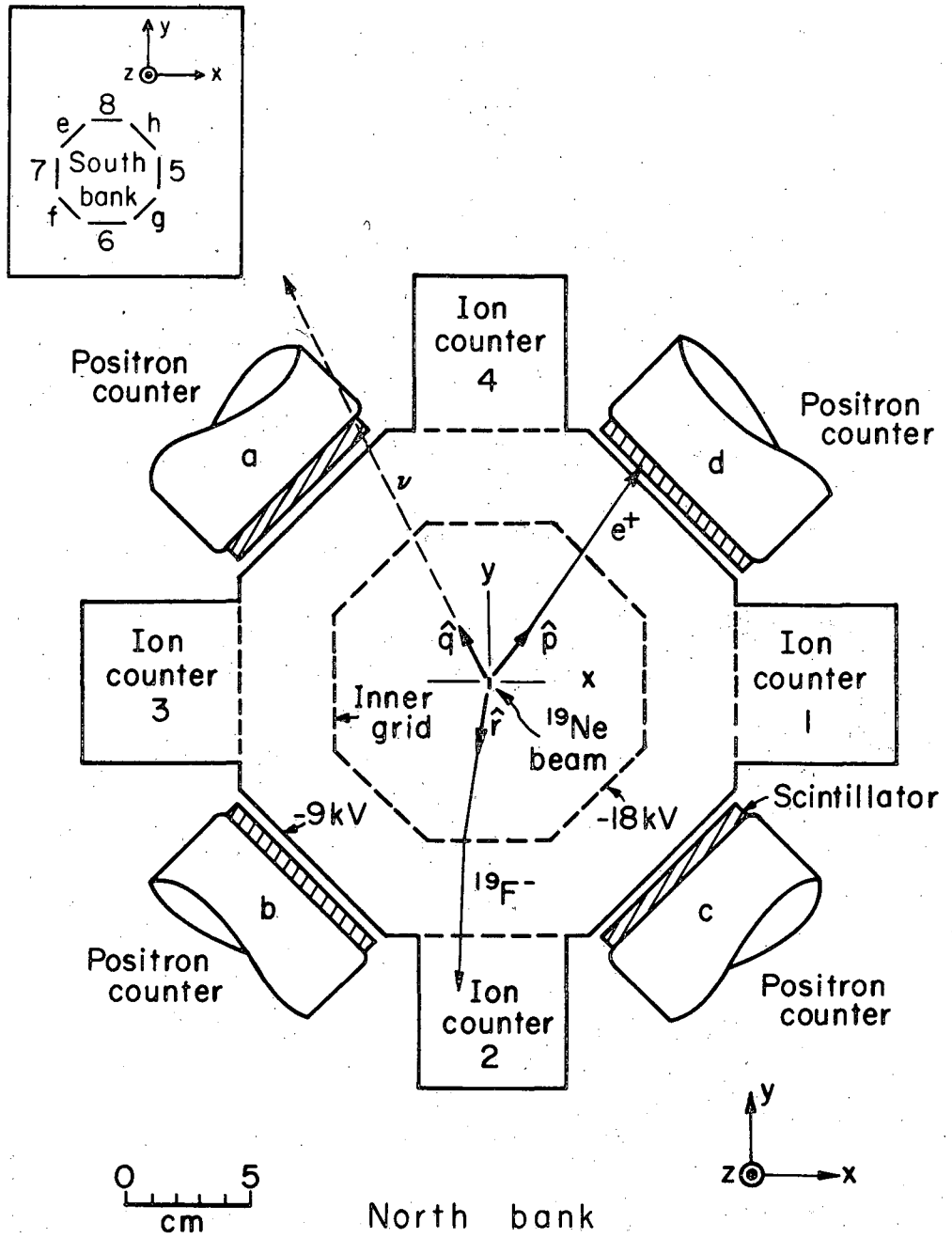
XBL691-1625

Fig. 2b



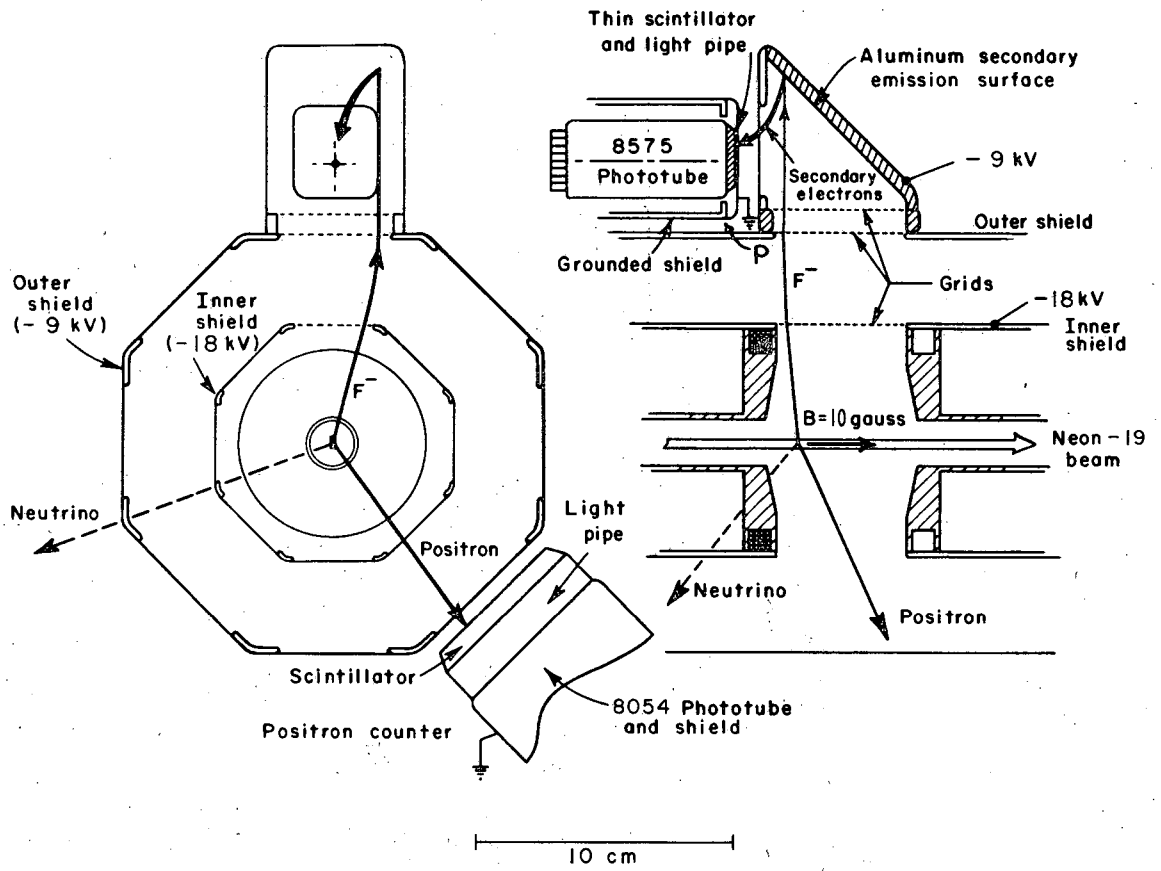
XBL691-1626

Fig. 2c



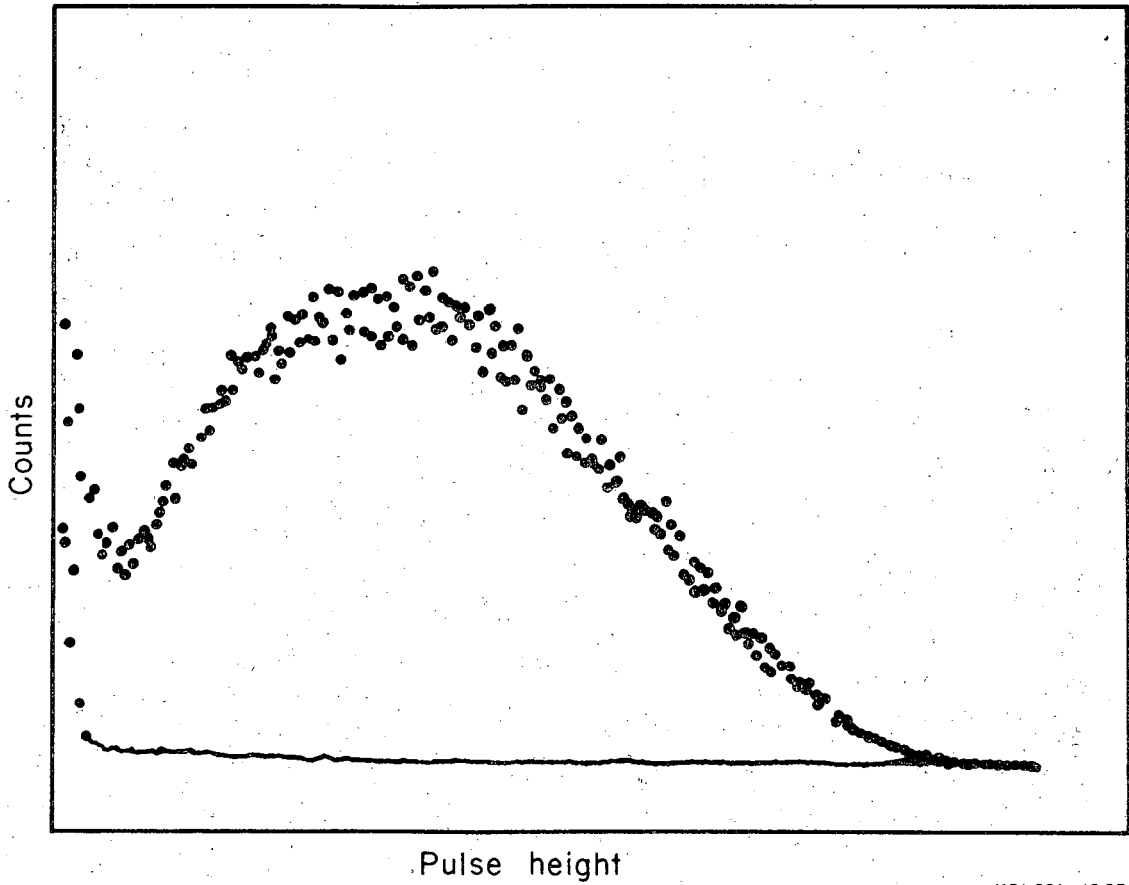
XBL673-2444-A

Fig. 3



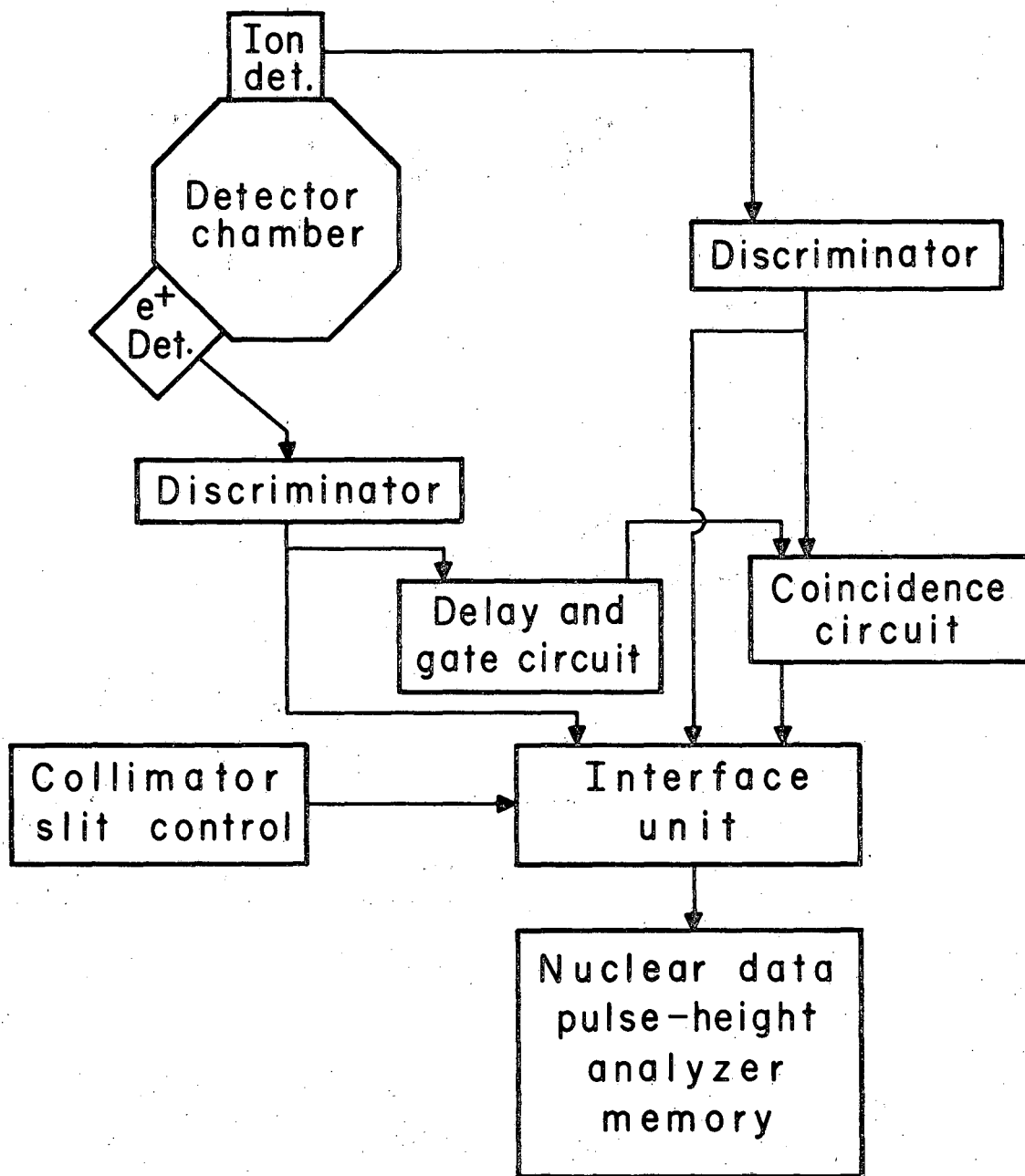
XBL671-115 A

Fig. 4



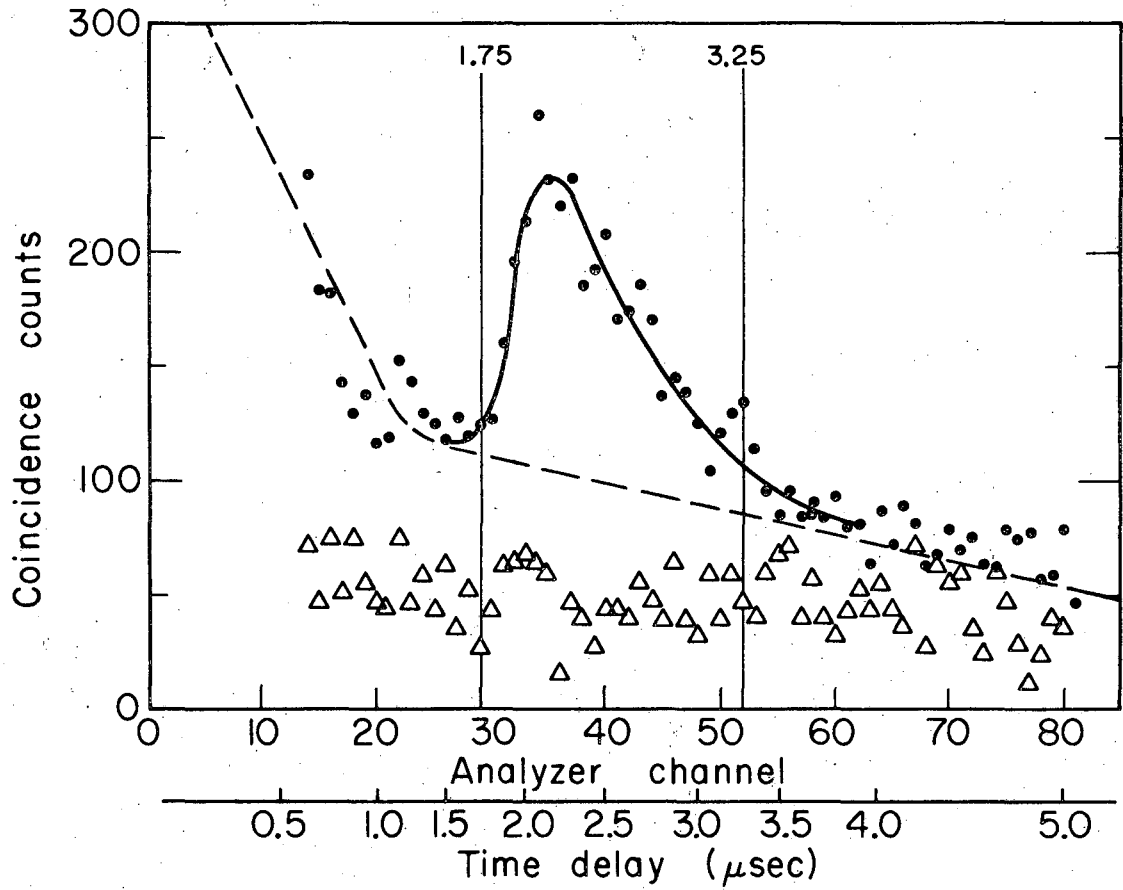
XBL691-1825

Fig. 5



XBL691-1624

Fig. 6



XBL691-1628

Fig. 7

LEGAL NOTICE

This report was prepared as an account of Government sponsored work. Neither the United States, nor the Commission, nor any person acting on behalf of the Commission:

- A. Makes any warranty or representation, expressed or implied, with respect to the accuracy, completeness, or usefulness of the information contained in this report, or that the use of any information, apparatus, method, or process disclosed in this report may not infringe privately owned rights; or*
- B. Assumes any liabilities with respect to the use of, or for damages resulting from the use of any information, apparatus, method, or process disclosed in this report.*

As used in the above, "person acting on behalf of the Commission" includes any employee or contractor of the Commission, or employee of such contractor, to the extent that such employee or contractor of the Commission, or employee of such contractor prepares, disseminates, or provides access to, any information pursuant to his employment or contract with the Commission, or his employment with such contractor.

TECHNICAL INFORMATION DIVISION
LAWRENCE RADIATION LABORATORY
UNIVERSITY OF CALIFORNIA
BERKELEY, CALIFORNIA 94720